Performance of a collimating L-shaped laterally graded multilayer mirror for the IXS analyzer system at NSLS-II

Alexey Suvorov,[a]* David S. Coburn,[a] Alessandro Cunsolo,[a] Jeffrey W. Keister,[a] Mary H. Upton[b] and Yong Q. Cai[a]

[a]Photon Sciences, Brookhaven National Laboratory, PO Box 5000, Upton, NY 11973, USA, and [b]Advanced Photon Source, Argonne National Laboratory, 9700 South Cass Avenue, Argonne, IL 60439, USA. *E-mail: asuvorov@bnl.gov

The L-shaped laterally graded multilayer mirror is a vital part of the ultrahigh-energy and momentum-resolution inelastic X-ray scattering spectrometer at the National Synchrotron Light Source II. This mirror was designed and implemented as a two-dimensional collimating optic for the analyzer system. Its performance was characterized using a secondary large-divergence source at the 30-ID beamline of the Advanced Photon Source, which yielded an integrated reflectivity of 47% and a collimated beam divergence of 78 µrad with a source size of 10 µm. Numerical simulations of the mirror performance in tandem with the analyzer crystal optics provided details on the acceptance sample volume in forward scattering and defined the technical requirements on the mirror stability and positioning precision. It was shown that the mirror spatial and angular stability must be in the range <8.4 µm and <21.4 µrad, respectively, for reliable operation of the analyzer.

1. Introduction

Inelastic X-ray Scattering (IXS) with meV energy resolution has been developed over the last decades into a powerful tool for studying vibrational dynamics and excitations in a variety of condensed-matter systems thanks to the advent of high brilliant synchrotron sources and the development of spherically bent backscattering crystal analyzers (Krisch & Sette, 2007). These analyzers combine mrad-level of angular acceptance with energy resolution close to the intrinsic width of the Bragg reflection used and have been instrumental in the enormous success of the technique. However, to pursue higher, sub-meV, resolutions, one has to use higher-order Bragg reflections that correspond to higher photon energies, which, in addition to many other disadvantages, is incompatible with the fact that undulator-based synchrotron sources generate much less flux in the high-energy spectral range while IXS is extremely flux limited. The ultrahigh-energy resolution IXS spectrometer being developed at the National Synchrotron Light Source II (NSLS-II) employs an innovative optical design that aims to circumvent this problem (Cai et al., 2013). Its analyzer system utilizes a multi-crystal arrangement, namely the so-called CDW scheme (Shvyd'ko, 2004), that explores the angular dispersion effect in extremely asymmetric Bragg reflections to achieve sub-meV energy resolution at a moderate energy of about 9.1 keV with high spectral

efficiency, which capitalizes on the superior performance of undulator sources of NSLS-II at this energy range. On the other hand, although its moderate angular acceptance (~0.1 mrad) is high compared with many other high-resolution multi-crystal monochromator designs, it is still about two orders of magnitude lower than the spherically bent back-scattering analyzers. The L-shaped laterally graded multilayer mirror to be discussed below is designed to improve the angular acceptance of this new analyzer optics to a comparable level.

Multilayer mirrors are basic optical elements of X-ray optics (Spiller, 2010). Application of a single multilayer mirror has so far been primarily limited to one-dimensional shaping of X-rays (Morawe & Osterhoff, 2010). For two-dimensional shaping of X-rays, such as in a focusing application, several mirrors are commonly combined into one optical set-up, e.g. as in the Kirkpatrick–Baez (KB) configuration (Kirkpatrick & Baez, 1948), where the two-dimensional shaping is performed sequentially for one dimension at a time. This circumvents the technical challenge of fabricating a multilayer mirror with aspherical surface figure. The obvious disadvantage of a multiple mirror set-up is that it requires additional instrumentation, space and stability control.

Despite the progress in the fabrication of aspherical multilayer mirrors with short focal distances (Wohlschlögel et al., 2008), some specific parameters of aspherical mirrors, such

473

as the mid-spatial frequency roughness, are still worse than their one-dimensional counterpart. Another approach to creating a single multilayer mirror with two-dimensional figuring is using the so-called L-shaped [also known as Montel (Montel, 1957) or nested] mirror. The L-shaped mirror combines two one-dimensionally figured multilayer mirrors attached at 90° to each other. In such an arrangement, X-rays are reflected in sequence by both mirrors simultaneously with the sequence depending on the spatial location of the X-rays (Honnicke *et al.*, 2010), which leads to a more efficient space usage and a more compact set-up. Furthermore, it retains the advantage of one-dimensional mirrors for better surface figuring, and can be designed as either a focusing (with elliptic figures) or collimating (with parabolic figures) device. Such type of mirrors as a focusing device has been tested with neutron (Ice *et al.*, 2009) and X-ray sources (Liu *et al.*, 2011; Honnicke *et al.*, 2011), and is already in use in commercial diffractometers (Hertlein *et al.*, 2005; Shymanovich *et al.*, 2008).

Here we present experimental characterization and numerical analysis of the collimating performance of an L-shaped multilayer mirror designed and built for the analyzer system of the ultrahigh-energy-resolution IXS spectrometer at NSLS-II. The mirror was manufactured by Incoatec GmbH (Innovative Coating Technologies GmbH). It was designed to collect at least 10 mrad of diverging beam from a 5 μm × 5 μm X-ray source at a distance of 200 mm from the mirror center, and collimate it to better than 0.1 mrad in both the vertical and horizontal directions. Each surface of the mirror has the same parabolic cylindrical figure with a graded multilayer coating. A detailed description of the mirror parameters along with metrology and point reflectivity measurements, and X-ray focusing performance, have been presented earlier (Honnicke *et al.*, 2010, 2011). Here the mirror collimating performance, efficiency and positioning stability requirements will be addressed.

2. Experiment

To evaluate the mirror collimating performance, a large-divergent X-ray source with small lateral dimensions is required at an operating energy of about 9.1 keV. This can be obtained using off-axis scattering of a monochromatic X-ray beam from a scatterer. The lateral dimensions of the source can be defined by a pinhole of the appropriate size installed downstream of the scatterer. The divergence of the collimated beam can be measured by the rocking curve width of a double-crystal analyzer in a (+,+) arrangement (Authier, 2001). As a first approximation the measured divergence of the beam after the mirror can be represented as a convolution of the divergence from a point source with the angular aperture of the source itself (as seen from the mirror center) and the angular resolution of the double-crystal analyzer. To measure the inherent collimation performance of the mirror, the contributions from the source angular aperture and analyzer angular resolution must be negligible.

The experiment was carried out at the 30-ID beamline of the Advanced Photon Source. The experimental set-up is schematically shown in Fig. 1. The incident beam energy was set at 9.177 keV by the beamline Diamond 111 double-crystal monochromator with an energy width of ∼0.6 eV. This monochromatic beam was focused onto a 2 mm-thick Plexiglas plate using the beamline KB mirror system. The measured beam dimensions at the plate were about 65 μm × 100 μm (V × H). The Plexiglas plate was used as a scatterer. The scattered X-rays were then passed through a 50 μm-thick tungsten pinhole placed 5 mm downstream from the Plexiglas plate. The pinhole was offset vertically from the incident beam axis which controlled the scattered radiation intensity and direction (scattering angle φ, Fig. 1). In the experiment a scattering angle $\varphi \simeq 2.4°$ was used. The pinhole plate also defined the dimension of the secondary source in the set-up and acted as a beam stop for the direct beam. The secondary source divergence was defined primarily by the incident beam size and the distance from the scatterer to the pinhole. In the vertical direction, this amounts to about 20 mrad.

The beam incident on the L-shaped mirror was collimated by a vertical slit. The slit allowed us to perform divergence analysis of a beam reflected by a selected part of the mirror, and reduce the effective source divergence in the vertical plane. The slit was installed approximately 100 mm downstream of the pinhole. To visualize the reflected beam, a removable X-ray camera (PIXIS-XF: 1024, Princeton Instruments) was placed between the mirror and double-crystal divergence analyzer.

The L-shaped mirror was mounted 45° sagittally (Fig. 1) in a helium-filled box, which protected the multilayer from possible radiation damage and contamination during pre-alignment with the intense monochromatic incident beam. The mirror was mounted on a two-axis goniometer with linear
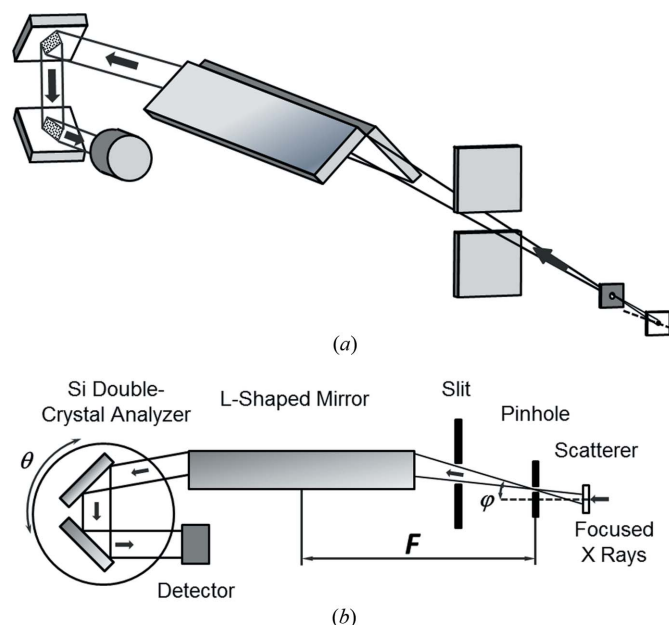

Figure 1
Sketch of the experiment set-up (see details in text).

Table 1
Divergence (FWHM) of the reflected beam measured with partial illumination of mirror aperture.

Slit size (mm)	Incident beam divergence (mrad)	Reflected beam divergence (µrad)
0.5	5	108.2
1.1	11	108.1
2.0	20	107.8

Figure 2
Rocking curve of the double-crystal analyzer (triangles) with the full illumination of the mirror aperture. The solid line is a Gaussian fit to the experimental data with a FWHM Δ_G = 107.8 µrad. The dashed line is a numerical simulation of the set-up with Δ_S = 108.1 µrad.

slides, which were used to align the mirror with the incoming beam. Since the mirror was oriented 45° sagittally, the overall reflection plane of the mirror was coplanar with the vertical plane, thus simplifying the alignment. The entrance and exit edges of the mirror had square apertures affixed (also rotated 45°) with dimensions of 2.3 mm and 3.2 mm, respectively. This limits the maximum vertical and horizontal angular acceptance of the mirror to about 20 mrad. The secondary source-to-mirror-center distance was set to F = 200 mm to match the design focal distance of the mirror (Fig. 1).

The double-crystal divergence analyzer was composed of two identical Si crystals in a (+,+) diffraction set-up. The crystals were aligned to the (440) reflections with an asymmetry angle of 19°. At the given energy the Si (440) Bragg angle was close to 45°. Thus, after two crystal reflections the reflected beam propagated in the direction opposite to the incident beam. The analyzer was set vertically with the diffraction plane of each crystal coplanar with the mirror reflection plane to measure the vertical divergence of the collimated beam. The intensity of the beam transmitted through the double-crystal analyzer was recorded with an avalanche photodiode detector. The theoretical full width at half-maximum (FWHM) of the analyzer resolution function was about 11.1 µrad.

In the first set of data the divergence of the collimated beam was measured *versus* the dimension of the virtual source which was defined by the pinhole size. For pinhole sizes of 10 µm, 25 µm and 50 µm, the measured divergence was 77.9 µrad, 120.7 µrad and 201 µrad, respectively. Subsequent data were collected with the 25 µm pinhole only. In the second set of data the source-to-mirror distance was optimized to minimize the divergence of the reflected beam measured by the analyzer. The position of the scatter-pinhole assembly was adjusted systematically and it was found that the minimum divergence occurred at a focal distance of $F \simeq$ 195 mm. Measurements were performed with partially closed slits upstream of the mirror, so that only the central part of the mirror was reflecting. Table 1 summarizes the reflected beam divergence measured with several slit openings at the 25 µm pinhole size.

It can be seen that the divergence of the collimated beam was improved compared with the one from the first data set. This can be attributed to the better mirror alignment and positioning. Negligible data spread in the collimated beam divergence at different slit openings (thus at different mirror illuminations) confirms the very good overall shape of the mirror. Fig. 2 illustrates the analyzer rocking curve measured with the slit opening of 2 mm. The intensity is fitted with a
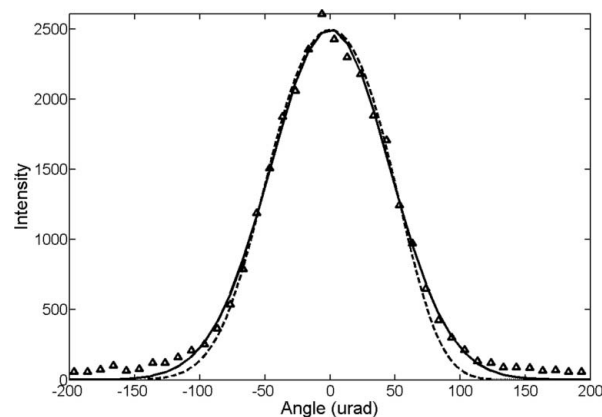
Gaussian curve and compared with simulation data. The simulation curve was calculated by ray tracing through the L-shaped mirror convoluting contributions from the double-crystal analyzer. The simulation also took into account the 25 µm pinhole aperture, the longitudinal slope error of 8.5 µrad r.m.s. of the mirror surface (Honnicke *et al.*, 2011), the theoretical reflectivity function width (0.7 mrad FWHM) of each mirror, and the dynamic diffraction rocking curve width of the crystal reflections of the divergence analyzer. The simulation is in agreement with the experimental results.

Fig. 3(*a*) presents an image of the reflected beam at a slit opening of 2 mm. It can be seen that the image is generally uniform, but has a periodic pattern in the directions normal to the mirror reflecting surfaces. The central vertical line in the image corresponds to the joint of the two substrates composing the L-shaped mirror. A slit opening of 2 mm provided full illumination of the mirror. Fig. 3(*b*) shows the Fourier transform of the image. There are four distinctive satellite peaks in the corners of a square with a distance $f \simeq$ 8.7 mm^{-1} from the center. Assuming an average angle of incidence of each mirror of about θ = 1.569°, the spatial period of the longitudinal surface modulation can be evaluated as $\Lambda = 1/f \sin\theta \simeq$ 4.2 mm along the mirror surface.

This observation is supported by the previously reported surface metrology data (Honnicke *et al.*, 2011) which revealed periodicity in surface slope error with a period of 4.22 mm.

Intensity measurements of the incident and reflected beams with full illumination of the mirror revealed a reflectivity value of $R \simeq$ 0.47 which agreed well with previous estimates (Honnicke *et al.*, 2011).

3. Simulations

As part of the analyzer system for the IXS spectrometer at NSLS-II, the L-shaped mirror is designed to collimate the scattered X-rays for further analysis by the high-energy-resolution crystal analyzer (Keister *et al.*, 2013; Cai *et al.*, 2013). Here we address the performance requirements of the
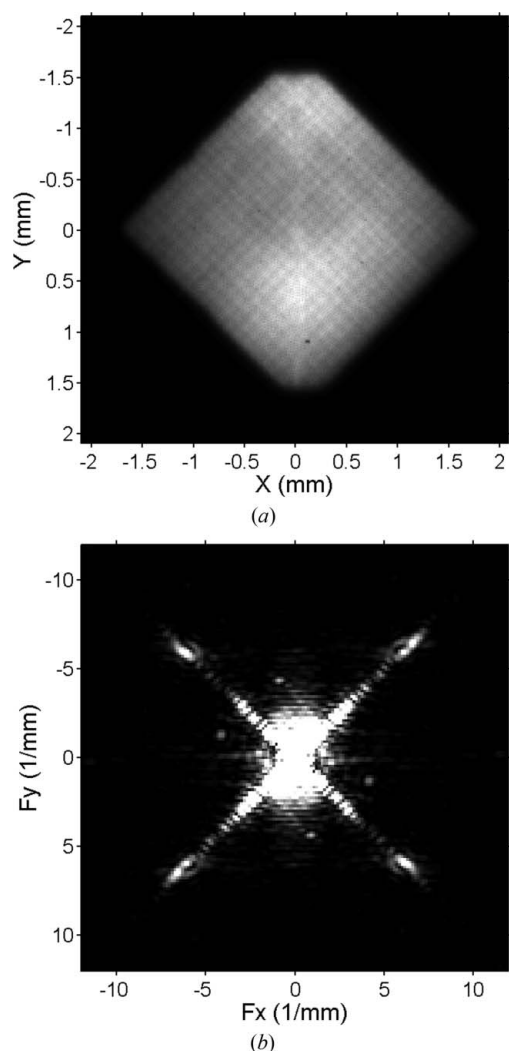
Figure 3
X-ray camera image of (*a*) the reflected beam and (*b*) its Fourier transform.

L-shaped mirror in tandem with the CDW crystal analyzer (Shvyd'ko, 2004; Cai *et al.*, 2013), which comprises three crystals acting as collimator, dispersing crystal and wavelength selector. The CDW analyzer acts as a spatial and angular filter on the beam collimated by the L-shaped mirror. The spatial acceptance of the CDW analyzer is limited by the length of the D crystal. An analyzer designed for 0.7 meV energy resolution requires a 1 m length of the D crystal to provide a maximum vertical acceptance of 1.2 mm. The vertical angular acceptance is limited by the rocking-curve width of the C crystal, which is about 106.5 µrad. The horizontal angular acceptance of the analyzer is limited by the allowable broadening of the analyzer energy resolution. In the case of 10% broadening, the horizontal angular acceptance should be limited to about 250 µrad.

Any spatial or angular deviation of the L-shaped mirror from its nominal position leads to intensity variation after the CDW analyzer. Thus, it is essential to understand the boundaries of these deviations and the system stability requirements. Our numerical simulations assume the following conditions:

(i) X-ray source of single wavelength with Gaussian intensity distribution and size of 5 µm FWHM diameter, (ii) ideal L-shaped laterally graded multilayer mirror with a focal distance F = 200 mm, and (iii) CDW analyzer placed at a distance of 5 m from the mirror and configured for 0.7 meV energy resolution. For each element in the set-up, a local Cartesian coordinate system is used, with the Z-axis directed along the incident X-ray beam, X-axis directed horizontally, and Y-axis directed vertically. Rotation of the mirror about the X-axis will be denoted as Theta-rotation and about the Y-axis as Phi-rotation. In the model, the mirror had a square entrance aperture of 2 mm × 2 mm with edges aligned along the mirror surfaces at 45° to the XY axes, and the CDW analyzer had a rectangular 3 mm × 1 mm ($X \times Y$) entrance aperture with edges aligned along the local X and Y directions. With the given square entrance aperture of the mirror, the maximum angular acceptance in the horizontal and vertical planes was about 20 mrad.

Fig. 4(*a*) shows a simulation of the intensity recorded after the CDW analyzer *versus* the linear displacement of the mirror in its local vertical (Y) and horizontal directions (X). FWHMs of the intensity profiles along these directions at maximum are Δ_X = 69.0 µm and Δ_Y = 14.5 µm.

The value of Δ_Y can be roughly evaluated from the set-up geometry: a change of the mirror vertical position by some value Δ leads to a change in the angle of incidence by $\delta \simeq \Delta/F$. In accordance with specular reflection, the reflected beam angle will be changed by the same amount. Taking into account the angular acceptance of the analyzer in the Y-direction, $\Delta\xi \simeq 100$ µrad, the maximum displacement range of the mirror is $\Delta_{\max} \simeq F\Delta\xi = 20$ µm.

Although such simulated numbers typically represent FWHMs of intensity profiles, stability requirements are
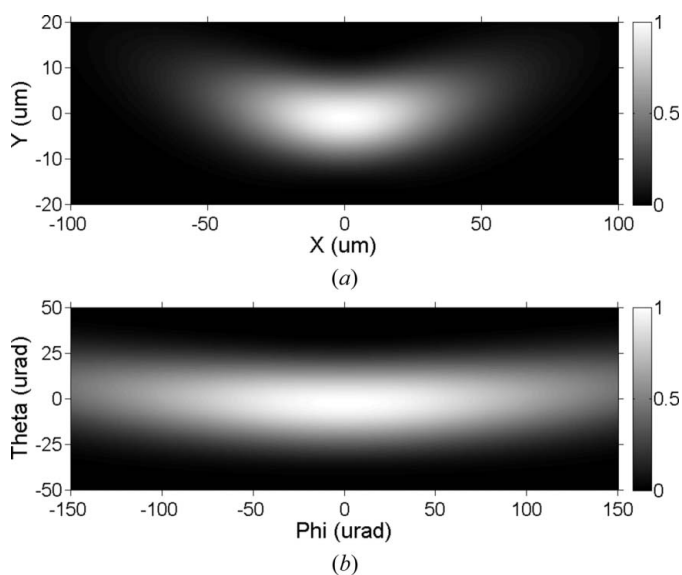

Figure 4
Simulation of the integrated intensity after the CDW analyzer *versus* (*a*) the linear displacement of the L-shaped mirror in the horizontal (X) and vertical (Y) directions, and (*b*) the angular rotation of the L-shaped mirror in the vertical (Theta) and horizontal (Phi) planes.

usually much tougher and call for maximum intensity variation within 10–20% from the maximum. The maximum allowable variation of the mirror vertical position in the case of a 20% margin is 8.4 µm. This is one of the most critical parameters for the IXS analyzer. The IXS spectrometer design envisions installation of the L-shaped mirror and CDW analyzer at the extremes of a 5 m-long arm which can be rotated around the sample. Maintaining the positions of the mirror and analyzer relative to each other with a high precision is a challenging task.

Fig. 4(b) shows a simulation of the integrated intensity *versus* variation of the mirror angular position. The angle Theta represents θ-rotation of the mirror (around the X-axis), and the angle Phi represents φ-rotation (around the Y-axis). FWHMs of the intensity profiles at maximum are $\Delta\varphi = 259.1$ µrad and $\Delta\theta = 36.8$ µrad. Once again a rough evaluation of $\Delta\theta$ can be obtained from the set-up geometry. A change of the angle of incidence by θ leads to a change of the reflected beam angle by 2θ. Taking into account the angular acceptance of the analyzer, $\Delta\xi \simeq 100$ µrad, the maximum variation of the mirror angle can be evaluated as $\Delta\theta_{max} \simeq \Delta\xi/2 = 50$ µrad. In terms of set-up stability, the maximum allowable variation of the mirror θ-position in the case of a 20% margin is 21.4 µrad.

We have also calculated the acceptance volume of the L-shaped mirror. Here we define the acceptance volume as the geometrical volume of source points which produce corresponding integrated intensity after the CDW analyzer. Thus, each point in the acceptance volume is associated with intensity transmitted through the mirror–analyzer system. The intersection of the acceptance volume of the mirror with the sample volume and the incident X-ray beam volume defines the scattering volume which can be analyzed by the analyzer system. Fig. 5(a) shows a three-dimensional surface defining a volume which contributes most (within 20% margin from maximum intensity) to the transmitted intensity. The volume is elongated along the direction of the incident beam, and its center is shifted upstream, towards longer distances to the mirror. This is caused by the fact that at distances longer than F the reflected beam becomes slightly focused and, thus, more intensity goes through the analyzer spatial aperture. Fig. 5(b) shows the intensity maps of the same acceptance volume sliced along the incident beam direction (Z). The FWHM values in the central part of the acceptance volume are $\sim$12.3 µm in the Y-direction and $\sim$65.7 µm in the X-direction.

4. Conclusion

An L-shaped laterally graded multilayer mirror was successfully tested in the collimation geometry using synchrotron radiation. The mirror demonstrated very good compliance with the design specification. The measured divergence of the collimated X-ray beam with the 10 µm pinhole was about 78 µrad. In the NSLS-II IXS spectrometer it is designed that the X-ray beam at the sample position will be focused down to 5 µm × 7 µm dimensions. It can be concluded that the collimated beam divergence will be well within 0.1 mrad of the angular acceptance of the crystal analyzer. The test proved
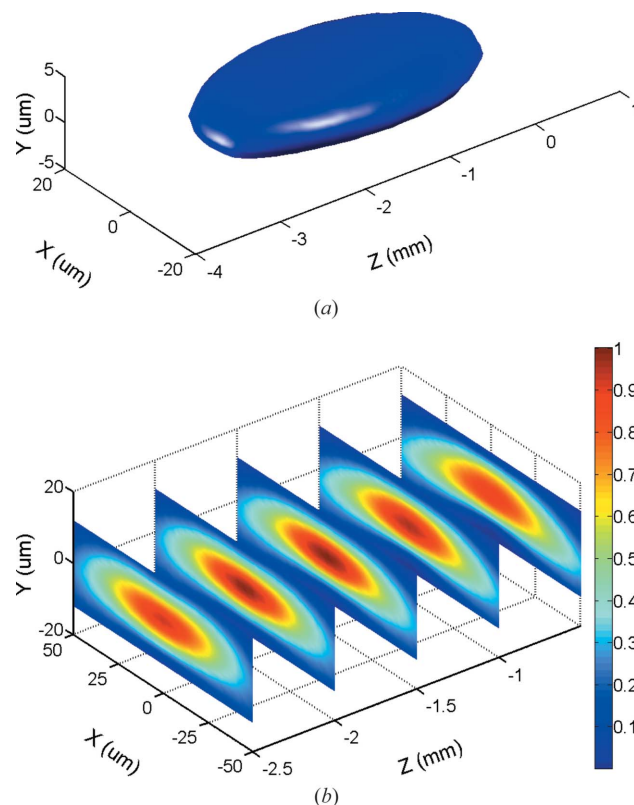

Figure 5
L-shaped mirror acceptance volume. Each point in the vicinity of mirror focal distance F is associated with an intensity transmitted through the mirror–analyzer system. (a) Three-dimensional surface containing points with intensity within 20% from the maximum. (b) Two-dimensional intensity slices of the acceptance volume along the incident beam direction.

that the L-shaped mirror will be a workable high-efficiency optical device in the IXS analyzer system.

Numerical simulations of the mirror performance in conjunction with the CDW analyzer revealed stringent requirements on the stability of relative positioning of the mirror with respect to the crystal analyzer, and of the mirror–crystal analyzer assembly with respect to the sample. The most critical parameter is the vertical positioning stability which should be maintained well within the 8 µm range.

References

Authier, A. (2001). *Dynamical Theory of X-ray Diffraction*. New York: Oxford University Press.
Cai, Y. Q., Coburn, D. S., Cunsolo, A., Keister, J. W., Honnicke, M. G., Huang, X. R., Kodituwakku, C. N., Stetsko, Y., Suvorov, A., Hiraoka, N., Tsuei, K. D. & Wille, H. C. (2013). *J. Phys. Conf. Ser.* **425**, 202001.
Hertlein, F., Oehr, A., Hoffmann, C., Michaelsen, C. & Wiesmann, J. (2005). *Part. Part. Syst. Charact.* **22**, 378–383.

Honnicke, M. G., Huang, X., Keister, J. W., Kodituwakku, C. N. & Cai, Y. Q. (2010). *J. Synchrotron Rad.* **17**, 352–359.

Honnicke, M. G., Keister, J. W., Conley, R., Kaznatcheev, K., Takacs, P. Z., Coburn, D. S., Reffi, L. & Cai, Y. Q. (2011). *J. Synchrotron Rad.* **18**, 862–870.

Ice, G. E., Pang, J. W. L., Tulk, C., Molaison, J., Choi, J.-Y., Vaughn, C., Lytle, L., Takacs, P. Z., Andersen, K. H., Bigault, T. & Khounsary, A. (2009). *J. Appl. Cryst.* **42**, 1004–1008.

Keister, J. W., Suvorov, A., Coburn, D. S., Cunsolo, A., Kodituwakku, C. N., Stetsko, Y. & Cai, Y. Q. (2013). *J. Phys. Conf. Ser.* **425**, 052032.

Kirkpatrick, P. & Baez, A. V. (1948). *J. Opt. Soc. Am.* **38**, 766–774.

Krisch, M. & Sette, F. (2007). *Inelastic X-ray Scattering from Phonons, Light Scattering in Solids IX: Novel Materials and Techniques*, pp. 317–370. Berlin: Springer Verlag.

Liu, W., Ice, G. E., Assoufid, L., Liu, C., Shi, B., Khachatryan, R., Qian, J., Zschack, P., Tischler, J. Z. & Choi, J.-Y. (2011). *J. Synchrotron Rad.* **18**, 575–579.

Montel, M. (1957). *X-ray Microscopy with Catamegonic Roof Mirrors, X-ray Microscopy and Microradiography*. New York: Academic Press.

Morawe, C. & Osterhoff, M. (2010). *X-ray Opt. Instrum.* **2010**, 479631.

Mundboth, K., Sutter, J., Laundy, D., Collins, S., Stoupin, S. & Shvyd'ko, Y. (2014). *J. Synchrotron Rad.* **21**, 16–23.

Shvyd'ko, Yu. (2004). *X-ray Optics, High-Energy-Resolution Applications*. Berlin: Springer.

Shymanovich, U., Nicoul, M., Sokolowski-Tinten, K., Tarasevitch, A., Michaelsen, C. & Von der Linde, D. (2008). *Appl. Phys. B*, **92**, 493–499.

Spiller, E. (2010). *Handbook of Optics*, Vol. 5, ch. 41, edited by M. Bass, C. DeCusatis, J. Enoch, V. Lakshminarayanan, G. Li, C. MacDonald, V. Mahajan and E. Van Stryland. New York: McGraw-Hill Professional.

Wohlschlögel, M., Schülli, T. U., Lantz, B. & Welzel, U. (2008). *J. Appl. Cryst.* **41**, 124–133.